Celal Bayar University Journal of Science

All-optical NOT, OR, and XOR Logic Gates Using Silicon Slot Waveguides

Semih Korkmaz[1]*

[1] Department of Computer Engineering, Bandirma Onyedi Eylul University, Balikesir 10200, Türkiye

* semihkorkmaz@bandirma.edu.tr
* Orcid No: 0000-0001-5576-7653

Received: 9 June 2024
Accepted: 9 September 2024
DOI: 10.18466/cbayarfbe.1498313

Abstract

All-optical NOT, OR, and Exclusive OR(XOR) logic gates utilizing silicon slot waveguides are proposed and numerically analyzed in this work. The structure has a silicon slab with slot regions such as two input waveguides and square cavity resonators and one output waveguide. The optical spectra of the designed structures are attained with the method of finite difference time domain. The all-optical logic gate features of the design are achieved by applying optical signals with 0^0 or 180^0 phase differences from the input ports. Basic parameters such as transmission spectrum (T), modulation depth (MD), and contrast ratio (CR) are performed to show the optical features and ability of the proposed logic gates. The threshold transmission limit is 1.7% to define the status of the output ports as ON or OFF. At 689.5 nm, the maximum transmission, modulation depth, and contrast ratio are 149%, 97%, and 15.36 dB, respectively.

Keywords: Optical logic gates, Silicon slot waveguides, Transmission spectrum.

1. Introduction

All-optical devices have enabled new improvements in photonic devices to transmit information along the optical channels with high efficiency [1-4]. To achieve this, the waveguide-based device is more commonly used [5-7]. There are main waveguide types like metal-insulator-metal waveguides [8,9], insulator-metal-insulator waveguides [10,11], metal slot waveguides [12], and dielectric slot waveguides [13]. Among these structures, dielectric waveguides are preferred due to their low power consumption, low cost, and high transmission efficiency [14-17]. By using dielectric slot waveguides, there are many research fields to optimize performances of optical-based devices in the last decade such as power splitters [18,19], Mach-Zehnder interferometers [20], logic gates [21], modulators [22] and sensors [23]. Dielectric or metal slot waveguide-based systems are frequently used to carry out the all-optical logic gates. Silicon slot waveguides are chosen with their lower propagation losses, and ease of fabrication features compared to the metal slot waveguides [24,25]. All-optical devices which are OR, NOT, and Exclusive OR(XOR) logic gates with silicon slot waveguides are numerically designed and analyzed in this work. The spectrum of transmission and magnetic fields distributions for the suggested all-optical logic devices are reached via the method of finite-difference time-domain (FDTD) with perfectly matched layer boundary conditions that are performed along the x- and y axes. Only one structure is utilized during all analyses. The study includes two basic stages. In the first stage, the ideal dimensions of the structure have been obtained by geometric parameter sweep analyses. In the second stage, numerical analyses of all-optical OR, XOR, and NOT logic devices are carried out without changing the dimensions of the structure. To demonstrate the structure's OR, XOR, and NOT logic gate functionalities, optical signals with either the 0^0 phase difference or 180^0 phase differences are transmitted through the silicon slot waveguides. When the OR logic gate is analyzed, the applied signals have the same phase. On the other hand, when XOR and NOT logic gates are examined, there are 0^0 or 180^0 phase differences for the applied input signals.

2. Materials and Methods

Figure 1 presents the design for all-optical OR, NOT, and XOR logic devices. This structure includes etched regions like waveguides and square resonators on the 100 nm-thick silicon plate. The depth of the etched regions is 100 nm. The main purpose of using a resonator in such

Celal Bayar University Journal of Science
Volume 20, Issue 3, 2024, p 84-90
Doi: 10.18466/cbayarfbe.1498313

systems is to enhance light at certain wavelengths and to adjust the resonance wavelengths by varying the geometric parameters of the resonators. Furthermore, utilizing resonators enables narrower resonances for specific ranges [26,27]. In that design, there are two input ports, one output port, and two identical and symmetrical square resonators. Palik model is used for the optical constants of the silicon [28]. The refractive index of the air is 1. Transverse magnetic polarized Gaussian sources are applied from the input ports. The logic 0 (OFF) or logic 1 (ON) states of the output are determined by the lowest level in the transmission. This is called threshold transmission. When the value of transmission is bigger than the limit of threshold transmission, the output is defined as logic 1 (ON). When the value of transmission is lower than the threshold transmission, the output is defined as OFF [29]. Lumerical Solutions solver based on the method of FDTD is used to attain the optical spectrum results of the designed structure [30]. The transmission values are obtained with the formula (1) [31]. P_{out} and P_{in} represent the powers at the output port and input port, respectively.

$$T = P_{out}/P_{in} \qquad (1)$$

The contrast ratio (CR) is another fundamental parameter for optical logic gates. It is calculated using the formula (2) [32].

$$CR(dB) = 10log\left(\frac{P_h}{P_l}\right) \qquad (2)$$

In this formula, P_h represents the minimum power value while the state of output is a logic high level (ON). P_l denotes the maximum power value as the state of output is a logic low level (OFF).

The modulation depth (MD) is the other basic parameter that is formulated using the expression (3) [29].

$$MD = \left(\frac{T|ON_{max} - T|OFF_{min}}{T|ON_{max}}\right) \times 100\% \qquad (3)$$

In this expression, $T|ON_{max}$ represents the maximum transmission for logic level 1, while $T|OFF_{min}$ denotes the minimum transmission for logic level 0. Table 1 shows the lengths of the proposed structure. To attain the optimal values of the structures, parameter sweep analyses have been performed in the first stage. To do this, the optical signal is sent from only input 1. Figure 2 presents the transmission spectrum for the refractive index change of the transmission medium. When the refractive index of the medium is increased from 1 (air) to 1.9 with a 0.3 step size, the transmission values decrease from 55% to 45%. During this analysis, the lengths given in Table 1 are used. Figure 3(a) presents the transmission spectrum for the parameter sweep of w_1. w_1 is the critical parameter for transmitted signals due to the thickness of the waveguides. w_1 is changed from 20 nm to 50 nm. When the w_1 increases, the transmission values increase from 26% to 55%. Figure 3(b) presents the transmission spectrum obtained by the w_2 parameter sweep. The transmission values show different levels when w_2 is increased from 75 nm to 90 nm.

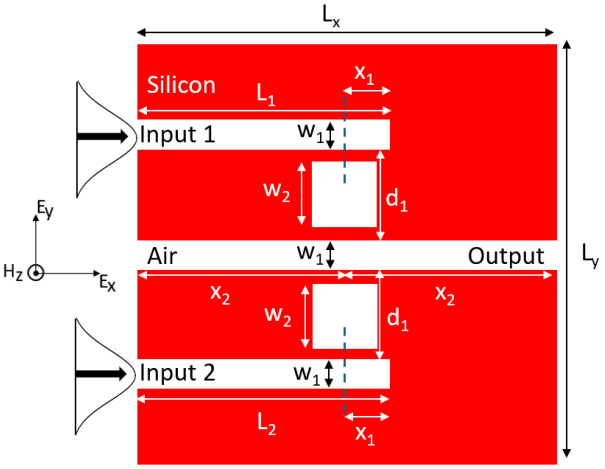

Figure 1. The illustration of the designed structure.

Table 1. The lengths of the proposed structure.

Parameter	Length (nm)
$L_X = L_Y$	400
$L_1 = L_2$	280
x_2	200
d_1	100
x_1	80
w_2	80
w_1	50

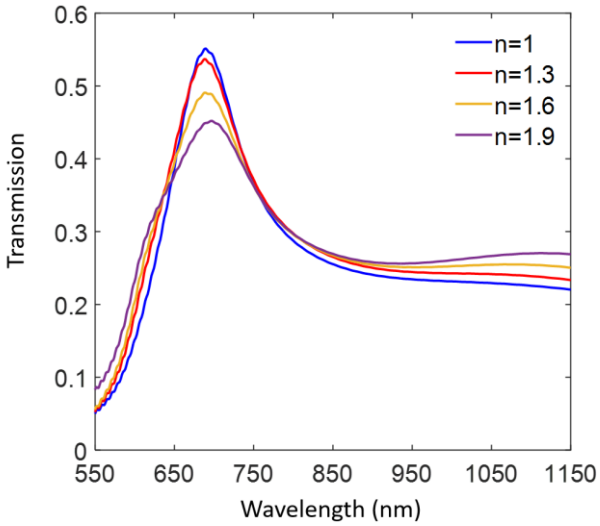

Figure 2. The transmission spectrum of the structure for different mediums.

The square design is obtained when w_2 is 80 nm, resulting in the highest transmission. Figure 3(c) visualizes the transmission spectrum from the variation of the x_1 parameter. x_1 is the important parameter for the transmitted signals due to the couplings between the

Celal Bayar University Journal of Science
Volume 20, Issue 3, 2024, p 84-90
Doi: 10.18466/cbayarfbe.1498313

waveguides and resonators. x_1 is changed from 20 nm to 80 nm. When the x_1 is increased, the transmission values increase from 36% to 55% at 689.5 nm. Figure 3(d) illustrates the transmission spectrum obtained from varying the parameter of x_2. When x_2 is increased from 140 nm to 200 nm, the transmission values increase from 30% to 55% at 689.5 nm. During the parameter sweeps, the lengths are constant except for the changed parameter. According to these analyses, the optimal lengths for w_1, w_2, x_1, and x_2 are defined as 50 nm, 80 nm, 80 nm, and 200 nm, respectively. Due to the structure limit of 400 nm × 400 nm, maximum length increments are reached in the parameter analyses in Figure 3. The structure remains consistent for all-optical logic gates during analyses. By adjusting the phases of the applied signal, three different logic gates can be achieved. To obtain higher transmission values, the refractive index of the medium for etched regions is 1 for the suggested all-optical logic gates.

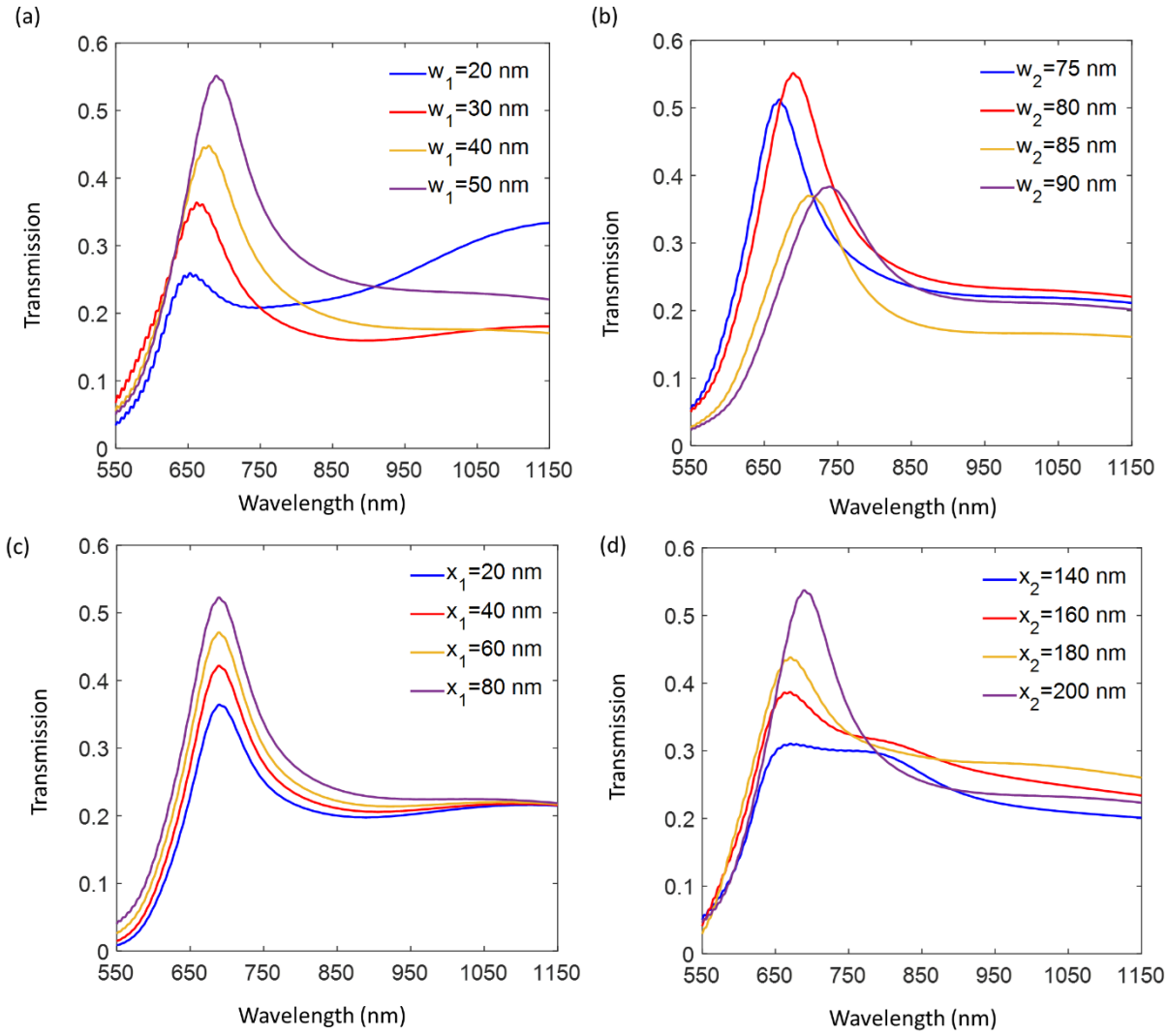

Figure 3. The transmission spectrum of the suggested structure for the sweep of (a) w_1, (b) w_2, (c) x_1, and (d) x_2.

3. Results and Discussion

3.1 Analysis of all-optical logic gates

3.1.1 Optical NOT gate

In the second stage, the first optical logic gate is a NOT gate. For that purpose, input 2 is used as a control port. During this analysis, logic 1 is applied from this port. When the signals are applied from the two ports, there are 180^0 phase differences between them. When the input 1 is logic 0 (OFF), the state of the output port is logic 1 (ON). As the input 1 is logic 1 (ON), the state of the output port is logic 0 (OFF) with a destructive interference effect. While all-optical logic gates are analyzed, constructive interference takes place if the signals are sent from the two ports in the same phase. The destructive interference occurs if the signals are applied in different phases [33,38]. Figure 4 visualizes the transmission spectrum of all-optical NOT gates. As given in Table 2, the values of transmission are 55% and 1.6% when input 1 is logic 0 and logic 1, respectively. Since

1.7% is threshold transmission, 55% and 1.6% present the status of the output ports as ON and OFF, respectively. According to the results obtained in this study, the threshold transmission value has been determined to be 1.7%, which is very low compared to values in the literature [34-38]. Transmission values higher than this threshold are considered logic 1, while values lower than it are considered logic 0. Figure 4 also presents the magnetic fields distributions at 689.5 nm when input 1 is logic 0 (blue line) and logic 1 (red dashed line). At 689.5 nm, the optical NOT gate demonstrates CR and MD values of 15.36 dB and 97%, respectively.

Table 2. The states of input 1 and input 2, the phase differences of the applied input signals, the transmission values, and the output states of all-optical NOT logic gate.

Input 1	Input 2 (Control port)	Phase Differences	Transmission (at 689.5 nm)	Output
Logic 0	Logic 1	0^0	55%	ON
Logic 1	Logic 1	180^0	1.6%	OFF

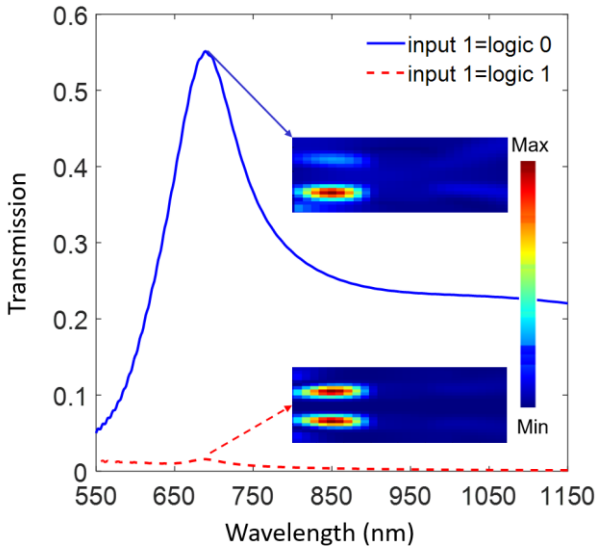

Figure 4. The spectrum of transmission and the magnetic fields distributions of suggested all-optical NOT gates for input 1=logic 0 and input 1=logic 1 at 689.5 nm.

3.1.2 Optical OR gate

The second logic gate is the all-optical OR gate. In this part, input 1 and input 2 are utilized to apply the input signals. During this analysis, the applied signals have the same phase. 01, 10, and 11 input signals are applied orderly from input 1 and input 2 as given in Table 3. Figure 5 visualizes the spectrum of transmission for the all-optical OR gate. When 01 and 10 are applied, the transmission value is 55%. When 11 is applied, the transmission value reaches its highest value of 149% with the constructive interference effect. In this analysis, all transmission values are higher than the threshold transmission value, resulting in ON output states. Figure 5 also illustrates the magnetic fields distributions for input 1=logic 0 and input 2=logic 1 (blue line), input 1=logic 1 and input 2=logic 0 (red dashed line), and input 1=logic 1 and input 2=logic 1 (brown dashed line) at 689.5 nm. When the transmission value increases, stronger modes are localized on the structure.

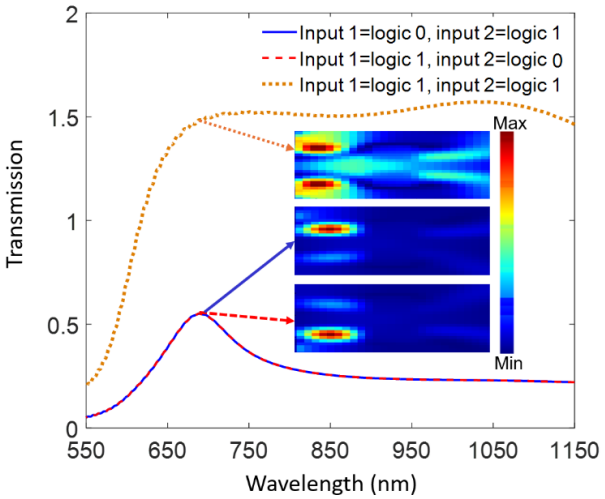

Figure 5. The spectrum of transmission and the magnetic fields distributions of suggested all-optical OR gates for input 1=logic 0 and input 2=logic 1, input 1=logic 1 and input 2=logic 0, and input 1=logic 1 and input 2=logic 1 at 689.5 nm.

Table 3. The states of input 1 and input 2, the phase differences of the applied input signals, the transmission values, and the output states of all-optical OR logic gate.

Input 1	Input 2	Phase Differences	Transmission (at 689.5 nm)	Output
Logic 0	Logic 1	0^0	55%	ON
Logic 1	Logic 0	0^0	55%	ON
Logic 1	Logic 1	0^0	149%	ON

3.1.3 Optical XOR gate

The third logic gate is the all-optical XOR gate. In this part, the input signals are applied from input 1 and input 2 as seen in Table 4. The signals have similar phases while the 01 and 10 input signals are sent. As the signals of 11 are applied, there is a 180° phase difference between the two input ports. Figure 6 illustrates the spectrum of transmission for the all-optical XOR gate. The values of transmission reach 55% when 01 and 10 are injected from the two input ports. The value of transmission is at the lowest level of 1.6% when 11 is applied with the effect of destructive interference. Since 1.7% is the threshold transmission value, output ports with 55% and 1.6% transmission represent the ON and OFF states, respectively. Figure 6 also visualizes the distributions of magnetic fields at 689.5 nm for input 1=logic 0 and input 2=logic 1 (blue line), input 1=logic 1 and input 2=logic 0 (red dashed line), and input 1=logic 1 and input 2=logic 1 (brown dashed line). When the transmission value is 55%, stronger modes are localized on the structure. Similar to the XOR gate, the optical NOT gate supports CR and MD values of 15.36 dB and 97%, respectively. This study generally demonstrates better results than previous studies in terms of the threshold transmission limit and transmission value, as shown in Table 5.

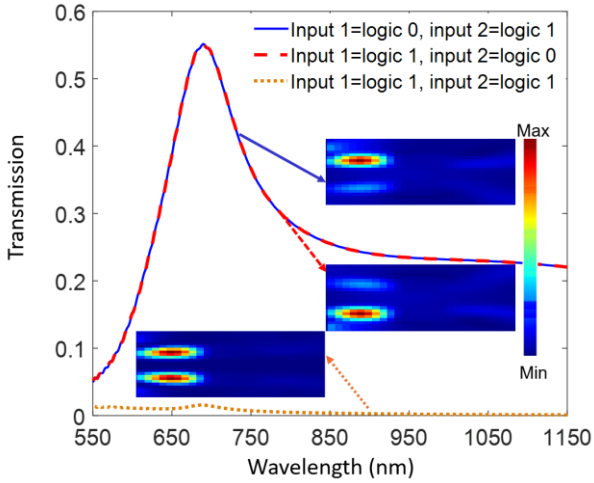

Figure 6. The spectrum of transmission and the magnetic fields distributions of all-optical XOR gates for input 1=logic 0 and input 2=logic 1, input 1=logic 1 and input 2=logic 0, and input 1=logic 1 and input 2=logic 1 at 689.5 nm.

Table 4. The states of input 1 and input 2, the phase differences of the applied input signals, the transmission values, and the output states of all-optical XOR logic gate.

Input 1	Input 2	Phase Differences	Transmission (at 689.5 nm)	Output
Logic 0	Logic 1	0^0	55%	ON
Logic 1	Logic 0	0^0	55%	ON
Logic 1	Logic 1	180^0	1.6%	OFF

Table 5. Comparison of the study with previously reported studies.

Reference	Number of designed optical logic gates	Transmission threshold value	The highest transmission	The highest contrast ratio (dB)
[34]	1	50%	73%	3.16
[35]	2	30%	69%	24.76
[36]	3	30%	78%	20.66
[37]	3	-	80%	25.86
[38]	4	20%	143%	28.75
This study	3	1.7%	149%	15.36

4. Conclusion

This work presents the results of all-optical OR, XOR, and NOT logic devices with silicon slot waveguides. The FDTD method is used to determine the spectra of transmission and distributions of magnetic fields for the structures. To reach the ideal geometrical lengths of the structure, parameter sweep analyses have been performed. The highest transmission value is 149% for optical OR logic gates. The maximum modulation depth and contrast ratio are 97% and 15.36 dB for optical NOT and XOR logic gates. The study presents valuable results in designing dielectric waveguide-based optical devices.

Author's Contributions

Semih Korkmaz: Designed the structure, performed the analysis, drafted and wrote the manuscript

Ethics

There are no ethical issues after the publication of this manuscript.

References

[1]. Chai, Z, Hu, X, Wang, F, Niu, X, Xie, J, Gong, Q. 2017. Ultrafast all-optical switching. *Advanced Optical Materials*; 5(7): 1600665.

[2]. Wang, X, Qi, H, Hu, X, Yu, Z, Ding, S, Du, Z, Gong, Q. 2021. Advances in photonic devices based on optical phase-change materials. *Molecules*; 26(9): 2813.

[3]. Wesemann, L, Davis, TJ, Roberts, A. 2021. Meta-optical and thin film devices for all-optical information processing. *Applied Physics Reviews;* 8(3): 031309.

[4]. Mohammadi, M, Habibi, F, Seifouri, M, Olyaee, S. 2022. Recent advances on all-optical photonic crystal analog-to-digital converter (ADC). *Optical and Quantum Electronics*; 54(3): 192.

[5]. Khonina, SN, Voronkov, GS, Grakhova, EP, Kazanskiy, NL, Kutluyarov, RV, Butt, MA. 2023. Polymer waveguide-based optical sensors—interest in bio, gas, temperature, and mechanical sensing applications. *Coatings*; 13(3): 549.

[6]. Wang, Z, Xu, X, Fan, D, Wang, Y, Subbaraman, H, Chen, RT. 2016. Geometrical tuning art for entirely subwavelength grating waveguide based integrated photonics circuits. *Scientific Reports*; 6(1): 24106.

[7]. Ferrando-Rocher, M, Herranz-Herruzo, JI, Valero-Nogueira, A, Baquero-Escudero, M. 2021. Half-mode waveguide based on gap waveguide technology for rapid prototyping. *IEEE Microwave and Wireless Components Letters*; 32(2): 117-120.

[8]. Singh, L, Zhu, G, Kumar, GM, Revathi, D, Pareek, P. 2021. Numerical simulation of all-optical logic functions at micrometer scale by using plasmonic metal-insulator-metal (MIM) waveguides. *Optics & Laser Technology*, 135: 106697.

[9]. Swarnakar, S, Reddy, SK, Harijan, R, Kumar, S. 2021. Design and modelling of all-optical NAND gate using metal–insulator–metal (MIM) waveguides-based Mach–Zehnder interferometers for high-speed information processing. *Optical and Quantum Electronics*; 53(9): 493.

[10]. Shnan, NS, Sadeghi, S, Farzaneh, M, Hamidi, SM, Belotelov, VI, Chernov, AI. 2022. Longitudinal magneto-optical Kerr effect in insulator/metal/insulator grating structure. *Journal of Superconductivity and Novel Magnetism;* 35(11): 3397-3401.

[11]. Jasim, WA, Ali, FM, Abdullah, AK, AbdulNabi, MA. 2021. Design and simulation of optical logic gates based on insulator-metal–insulator (IMI) plasmonic waveguides for optical communications. *International Journal of Nonlinear Analysis and Applications*; 12(2): 2483-2497.

[12]. Dionne, JA, Lezec, HJ, Atwater, HA. 2006. Highly confined photon transport in subwavelength metallic slot waveguides. *Nano Letters*; 6(9): 1928-1932.

[13]. Su, R, Tang, D, Ding, W, Chen, L, Zhou, Z. 2011. Efficient transmission of crossing dielectric slot waveguides. *Optics Express;* 19(5): 4756-4761.

[14]. Mashanovich, GZ, Gardes, FY, Thomson, DJ, Hu, Y, Li, K, Nedeljkovic, M., Penades JS, Khokhar, AZ, Mitchell, CJ, Stankovic S, Topley R, Reynolds, SA, Wang, Y, Troia, B, Passaro, VMN, Littlejohns, CG, Bucio, TD, Wilson PR, Reed, GT. 2014. Silicon photonic waveguides and devices for near-and mid-IR applications. *IEEE Journal of Selected Topics in Quantum Electronics*; 21(4): 407-418.

[15]. Dhingra, N, Dell'Olio, F. 2020. Ultralow loss and high extinction ratio TM-pass polarizer in silicon photonics. *IEEE Photonics Journal*; 12(6): 1-11.

[16]. Sun, L, Zhang, Y, He, Y, Wang, H, Su, Y. 2020. Subwavelength structured silicon waveguides and photonic devices. *Nanophotonics*; 9(6): 1321-1340.

[17]. Su, Y, Zhang, Y, Qiu, C, Guo, X, Sun, L. 2020. Silicon photonic platform for passive waveguide devices: materials, fabrication, and applications. *Advanced Materials Technologies*; 5(8): 1901153.

[18]. Malka, D, Danan, Y, Ramon, Y, Zalevsky, Z. 2016. A photonic 1×4 power splitter based on multimode interference in silicon–gallium-nitride slot waveguide structures. *Materials;* 9(7): 516.

[19]. Nikolaevsky, L, Shchori, T, Malka, D. 2018. Modeling 1×8 MMI Green Light Power Splitter Based on Gallium-Nitride Slot Waveguide Structure. *IEEE Photonics Technology Letters;* 30(8): 720-723.

[20]. Sarkar, D, Jamal, I, Mitra, SK. 2013. Analysis, design and fabrication of optical waveguides for Mach–Zehnder Interferometry. *Optics Communications*; 311: 338-345.

[21]. Yu, R, Zhang, J, Chen, W, Wang, P, Li, Y, Li, J, Qiang F, Tingge D, Hui Y, Yang, J. 2021. Optical reversible logic gates based on graphene-silicon slot waveguides. *Optik*; 228: 166182.

[22]. Rutirawut, T, Talataisong, W, Gardes, FY. 2021. Designs of silicon nitride slot waveguide modulators with electro-optic polymer and the effect of induced charges in Si-substrate on their performance. *IEEE Photonics Journal*; 13(2): 1-15.

[23]. Chiang, LY, Wang, CT, Lin, TS, Pappert, S, Yu, P. 2020. Highly sensitive silicon photonic temperature sensor based on liquid crystal filled slot waveguide directional coupler. *Optics Express*; 28(20): 29345-29356.

[24]. Lipson, M. 2005. Guiding, modulating, and emitting light on silicon-challenges and opportunities. *Journal of Lightwave Technology*; 23(12): 4222-4238.

[25]. Simili, DV, Cada, M. 2019. Low loss slow light propagation in silicon slot waveguide. *Optics Express;* 27(18): 26203-26217.

[26]. Qin, W, Liu, J, Yang, WW, Chen, JX, Li, Y, Xu, RL. 2021. Integrated-designs of filtering circuits based on adjustable dielectric waveguide resonators. *IEEE Transactions on Circuits and Systems II: Express Briefs*; 69(2): 284-288.

[27]. Korkmaz, S. 2024. Design and analysis of high performance 1×N optical wavelength demultiplexers based on MIM waveguide with polygon resonators. *Optical and Quantum Electronics*; 56(7): 1219.

[28]. Palik, ED. Handbook of optical constants of solids. Academic Press, 1998; pp 565-566.

[29]. Abdulwahid, SH, Wadday, AG, Abdulsatar, SM. 2023. Design of optical combinational circuits utilized with hybrid plasmonic waveguides. *Plasmonics*; 18(1): 9-28.

[30]. Lumerical FDTD Solutions, www.lumerical.com.

[31]. Korkmaz, S. 2024. Multiple ultra-narrow band-stop filters based on MIM plasmonic waveguide with nanoring cavities. *Physica Scripta*; 99(3): 035503.

[32]. Anagha, EG, Jeyachitra, RK. 2022. Optimized design of an all-optical XOR gate with high contrast ratio and ultra-compact dimensions. *Applied Physics B*; 128(2): 21.

[33]. Choi, D, Shin, CK, Yoon, D, Chung, DS, Jin, YW, Lee, LP. 2014. Plasmonic optical interference. *Nano Letters*; 14(6): 3374-3381.

[34]. Fakhruldeen, HF, Mansour, TS. 2020. Design of plasmonic NOT logic gate based on insulator–metal–insulator (IMI) waveguides. *Advanced Electromagnetics;* 9(1): 91-94.

[35]. Mainka, Sharma, S, Zafar, R, Mahdieh, MH, Singh, G, Salim, M. High contrast ratio based all-optical OR and NOR plasmonic logic gate operating at E band. In Optical and Wireless Technologies: Proceedings of OWT 2018, Singapore, 2020, pp 325-332.

[36]. Zafar, R, Nawaz, S, Salim, M. 2018. Fano resonance excited all-optical XOR, XNOR, and NOT gates with high contrast ratio. *Plasmonics*; 13(6): 1987-1994.

[37]. Dolatabady, A, Granpayeh, N. 2017. All-optical logic gates in plasmonic metal–insulator–metal nanowaveguide with slot cavity resonator. *Journal of Nanophotonics*, 11(2): 026001-026001.

[38]. El Haffar, R, Mahboub, O, Farkhsi, A, Figuigue, M. 2022. All-optical logic gates using a plasmonic MIM waveguide and elliptical ring resonator. *Plasmonics*; 17: 831–842.